Scaling and asymmetry in an electromagnetically forced dipolar flow structure

M. Duran-Matute, R. R. Trieling, and G. J. F. van Heijst
Department of Applied Physics & J.M. Burgers Center, Eindhoven University of Technology, P. O. Box 513, 5600 MB Eindhoven, The Netherlands

(Received 12 July 2010; revised manuscript received 7 September 2010; published 26 January 2011)

A dipolar flow structure is experimentally studied in a layer of salt solution driven by time-independent electromagnetic forcing. In particular, the response of the flow to the forcing is quantified by measuring the Reynolds number Re as a function of the Chandrasekhar number Ch (the ratio of Lorentz forces to viscous forces) and δ (the ratio of vertical to horizontal length scales of the flow domain). In agreement with theoretical predictions, two scaling regimes are found: $\mathrm{Re} \sim \mathrm{Ch}/\pi^2$ (viscous regime) and $\mathrm{Re} \sim \mathrm{Ch}^{1/2}\delta^{-1}$ (advective regime). The transition between the two regimes at $\mathrm{Ch}^{1/2}\delta \sim \pi^2$ is reflected in the flow geometry in the form of an asymmetry of the dipolar flow structure.

DOI: 10.1103/PhysRevE.83.016306 PACS number(s): 47.32.C−, 47.65.−d

I. INTRODUCTION

Electromagnetic (EM) forcing of conducting fluids is nonintrusive, and for this reason it is an unparalleled tool for the study of a large variety of flows. In particular, EM forcing has been used in shallow layers of electrolytes to study quasi-two-dimensional turbulence [1,2], shallow vortices [3], stability of shear flows [4], fully controllable multiscale flows [5], and the principles of stretching and folding in quasi-two-dimensional flows [6]. In addition, research of this type of forcing has been motivated by its applications on EM mixing and stirring in metallurgy [7] and the enhancement of turbulent heat transfer [8].

Due to the many uses of EM forcing, it is of interest to characterize the response of the flow to the forcing. In the case of a shallow layer of electrolyte, Bondarenko *et al.* [9] considered, in the first reported experiments of this kind, that the induced fluid velocity is proportional to the magnitude of the EM forcing. Tabeling *et al.* [10] also observed a linear dependence but only up to a well-defined forcing threshold. Above this threshold, it was observed that the rate of increase of the velocity with the forcing is smaller. Despite its limitations at relatively strong forcing magnitudes, the linear relationship has been used in many theoretical studies; see, e.g., Refs. [11,12].

In more recent experiments on a system of four vortices, the maximum velocity was measured as a function of the forcing, and it was found that the deviations from the linear dependence were small [13]. However, the same experimental data were recently reanalyzed [14], and for relatively high forcing magnitudes, the maximum velocity seemed to scale with the forcing to the power 2/3 rather than linearly; the latter behavior is in agreement with theoretical results where secondary motions and different vertical velocity profiles were taken into account. Figueroa *et al.* [15] examined the structure of a laminar dipolar vortex driven by a time-independent EM force in a shallow layer of electrolyte. They observed that the maximum velocity in the flow as a function of the forcing magnitude fits a second order polynomial. However, no physical reason was given for such a fit.

It is the aim of the present article to determine experimentally the scaling of the magnitude of the flow velocity in a shallow layer of electrolyte forced electromagnetically as a function of the relevant parameters: the forcing magnitude (which is characterized by the Chandrasekhar number Ch) and the aspect ratio δ of the depth to the horizontal scale of the flow. In contrast with previous studies, we extend the parameter regime to large forcing magnitudes and focus on the underlying physical mechanisms associated with the different flow behaviors. We quantify the response of the flow by measuring the horizontal velocity field of a simple electromagnetically forced flow—a dipolar flow structure—while exploring the parameter space. Two well-defined regimes were observed: the linear regime discussed previously and a regime where the velocity scales with the magnitude of the forcing to the power 1/2. Furthermore, it is found that the flow depends only on the parameter $\mathrm{Ch}\delta^2$ for the whole range of parameters studied.

The article is organized as follows. The experimental setup is described in Sec. II. Section III is devoted to the dimensional analysis of the problem. Section IV presents the experimental results. Then, in Sec. V, the implications for previous and future work are discussed, and finally, the conclusions are outlined in Sec. VI.

II. EXPERIMENTAL SETUP

The experimental setup consists of a water tank with a base of 30×50 cm^2, which is filled with a salt solution with a concentration of 178 g/l to a depth H and covered with a transparent perspex lid to avoid free-surface deformations (Fig. 1). To force the flow, two titanium electrodes (coated with Ir-MMO) are placed along two opposite sides of the tank, and three $28 \times 10 \times 1$ cm^3 rectangular permanent magnets are placed 1.1 cm underneath the tank bottom. The electrodes are placed in compartments which are connected to the measurement area of the tank by a system of thin horizontal slits through which the electric current easily passes. The system of slits isolates the chemical reaction products generated at the electrodes from the flow to be studied. As shown in Fig. 2, the magnet at the center has its north pole facing up, while the two side magnets have their north pole facing down. A constant electric current is applied through the fluid using a power supply with a precision of 10^{-2} A. Due to the interaction of the electric current and the magnetic field of the magnets, a Lorentz force,

$$\boldsymbol{F} = \boldsymbol{J} \times \boldsymbol{B}, \tag{1}$$

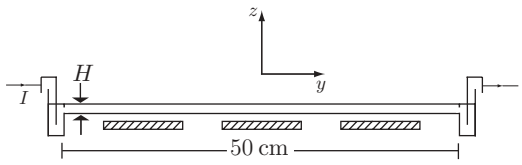

FIG. 1. Side view of the experimental setup. The hatched rectangles denote the magnets below the tank.

is generated (with $\boldsymbol{J}$ the current density and $\boldsymbol{B}$ the magnetic field), by which the fluid is set in motion.

We define a Cartesian coordinate system $\boldsymbol{x} = (x, y, z)$ with the origin at the center of the tank, x running parallel to the electrodes, y across the tank between the electrodes, and z in the vertical direction. Furthermore, we define the flow velocity $\boldsymbol{v} = (u, v, w)$. We consider the electric current to be homogeneous and running only in the y direction, while the main component of the magnetic field is in the z direction. Hence, the principal component of the Lorentz force is in the x direction. To characterize the fluid, we consider two of its properties: the kinematic viscosity $\nu = 1.544 \times 10^{-6}$ m^{2}s^{-1} [16] and the density $\rho = 1190$ kg m^{-3}, which are kept constant for the experiments reported here.

We consider three characteristic length scales of the flow: the length of the tank in the x direction, $L_x = 30$ cm, the distance between the centers of the two lateral magnets, $L_y = 30$ cm, and the depth of the fluid H, which was varied for different experiments, taking the values $H = 1.2$, 2.0 or 3.2 cm. The magnitude of the Lorentz force is characterized by $[\boldsymbol{J} \times \boldsymbol{B}] = IB/(L_x H)$, where the brackets denote the order of magnitude, I is the magnitude of the electric current through the fluid, and B is the magnitude of the magnetic field at mid-depth above the center of each magnet.

Particle image velocimetry (PIV) was used to measure the horizontal velocity field of the flow in a plane at mid-depth. The fluid was seeded with 106–150 μm polymethylmethacrylate (PMMA) particles which were illuminated at mid-depth with a double pulsed Nd:YAG laser sheet. Images of the central 30×30 cm^2 area of the tank (see Fig. 2) were taken, using a Megaplus ES 1.0 camera, at different time intervals (ranging from 10 ms to 1.3 s) depending on the maximum velocity

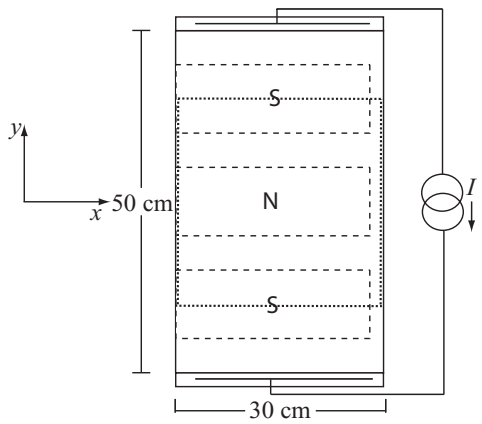

FIG. 2. Top view of the experimental setup. The dashed lines represent the position of the three magnets, and the dotted lines represent the limits of the measurement area.

in the flow. These images were then cross-correlated using PIV software from PIVTEC GmbH, Göttingen, Germany, to calculate the horizontal velocity field.

To characterize the response of the flow, we focus on the velocity in the x direction—i.e., in the direction of the principal component of the forcing—at $y = 0$. From now on, we refer to this velocity distribution as $\tilde{u}(x)$ which, as we shall see, corresponds to the velocity distribution along the symmetry axis of the dipolar structure at $y = 0$. Furthermore, we consider the mean value of this distribution

$$\langle \tilde{u}(x) \rangle \equiv \frac{1}{L_x} \int_{-L_x/2}^{L_x/2} \tilde{u}(x)\, dx \tag{2}$$

as the characteristic velocity scale.

III. DIMENSIONAL ANALYSIS

Dimensional analysis shows that four independent dimensionless parameters can be defined for this flow problem. The geometry of the tank is represented by two aspect ratios:

$$\delta \equiv \frac{H}{L_x} \quad \text{and} \quad \delta_L \equiv \frac{L_x}{L_y}, \tag{3}$$

whereas the Chandrasekhar number

$$\mathrm{Ch} \equiv \frac{IBH}{\rho \nu^2} \tag{4}$$

characterizes the forcing and represents the ratio of the Lorentz force to the viscous force. Note that the definition of Ch introduced here differs from the one originally used by Chandrasekhar [17]. In the original definition, the current density $\boldsymbol{J}$ is considered to be primarily driven by $\boldsymbol{v} \times \boldsymbol{B}$ in Ohm's law, but in the present work, $\boldsymbol{J}$ is given by $\boldsymbol{J} = I/(L_x H)\hat{\boldsymbol{j}}$ (with $\hat{\boldsymbol{j}}$ the unit vector in the y direction) since the induced effects can be neglected and the imposed Lorentz force dominates in electrolytes [15]. This is not the case for other conductive fluids such as liquid metals (see, e.g., Ref. [18]).

A similar definition for the ratio of Lorentz to viscous forces (4) is commonly referred to as *the Reynolds number based on the external force* (see, e.g., Ref. [19]). However, the term *Reynolds number* is reserved in this study for the parameter characterizing the response of the flow, which is here defined as

$$\mathrm{Re} \equiv \frac{\langle \tilde{u} \rangle L_x}{\nu}, \tag{5}$$

with $\langle \tilde{u} \rangle$ as the mean velocity and which represents the ratio of inertia forces to viscous forces.

In the experiments, the aspect ratio δ was set by the depth of the fluid, yielding the values $\delta = 0.040$, 0.067, and 0.107. For each value of δ, the Chandrasekhar number Ch was varied by changing the magnitude of the electric current. The magnitude of the magnetic field at mid-depth above the center of each magnet B then takes the values $B = 0.018$, 0.017, and 0.015 T for the different values of δ, respectively. In the experiments described here, the horizontal aspect ratio $\delta_L = 1$ is kept constant.

We consider the flow to be governed by the Navier-Stokes equation including the Lorentz force

$$\rho \frac{\partial \boldsymbol{v}}{\partial t} + \rho(\boldsymbol{v} \cdot \nabla)\boldsymbol{v} = -\nabla p + \rho \nu \nabla^2 \boldsymbol{v} + \boldsymbol{J} \times \boldsymbol{B}, \tag{6}$$

where p is the pressure. From here on, the first term will be neglected since the flow is stationary in the range of parameters studied.

To analyze the possible balances of forces in the flow, we consider the order of magnitude of each term in (6), where the pressure term is considered to be of the same order as the largest term in the equation. From this analysis, two different regimes are obtained.

A. Viscous regime

Due to the small depth, and hence, the predominance of friction at the bottom and the lid, we assume initially a Poiseuille-like vertical profile for the horizontal velocity field, i.e.,

$$u(x,y,z) = u^*(x,y)\sin\left(\frac{\pi z}{H}\right), \tag{7}$$

where $\sin(\pi z/H)$ is the first term of the Fourier expansion of a Poiseuille profile. In this way, the order of magnitude of the viscous force is given by

$$[\rho\nu\nabla^2\boldsymbol{v}] \approx \left[\rho\nu\frac{\partial^2\boldsymbol{v}}{\partial z^2}\right] \sim \frac{\pi^2\rho\nu\langle\tilde{u}\rangle}{H^2}, \tag{8}$$

considering that $\partial/\partial z \gg \partial/\partial x$.

The magnitude of the Lorentz force is given by

$$[\boldsymbol{J}\times\boldsymbol{B}] = \frac{IB}{L_x H}, \tag{9}$$

as mentioned before.

For relatively weak forcing and correspondingly small Reynolds numbers, inertia can be neglected, and the dominant balance is between the Lorentz and the viscous forces, i.e.,

$$\frac{IB}{L_x H} \sim \frac{\pi^2\rho\nu\langle\tilde{u}\rangle}{H^2}, \tag{10}$$

which is equivalent to

$$\mathrm{Re} \sim \frac{\mathrm{Ch}}{\pi^2}. \tag{11}$$

B. Advective regime

The order of magnitude of the advective term is given by

$$[(\boldsymbol{v}\cdot\nabla)\boldsymbol{v}] \sim \frac{\langle\tilde{u}\rangle^2}{L_x}, \tag{12}$$

where the velocity is considered to be of order $\langle\tilde{u}\rangle$ and L_x is taken as the characteristic length scale since advection takes place mainly in the horizontal plane.

For relatively strong forcing and correspondingly large Reynolds numbers, we may assume that the Lorentz force is of the same order as the inertia forces, so

$$\frac{IB}{L_x H} \sim \rho\frac{\langle\tilde{u}\rangle^2}{L_x}, \tag{13}$$

which is equivalent to

$$\mathrm{Re} \sim \frac{\mathrm{Ch}^{1/2}}{\delta}. \tag{14}$$

In addition, we should recall that the flow is stationary, and hence, the input of energy due to the forcing has to be balanced by viscous dissipation. This means that the viscous forces in (6) must be also of the same order as the Lorentz forces, which cannot be achieved if the velocity has a Poiseuille-like vertical profile. That is, the presumption of (7) that the vertical gradient of the velocity is proportional to $\langle\tilde{u}\rangle/H$ is not valid in the advective regime. Hence, we assume that the velocity varies on a scale h such that

$$[\nu\nabla^2\boldsymbol{v}] \approx \left[\frac{\nu}{h^2}\frac{\partial^2\boldsymbol{v}}{\partial z'^2}\right] \sim \frac{\nu\langle\tilde{u}\rangle}{h^2}, \tag{15}$$

where $z' = z/h$ and $h < H/\pi$. Finally, the balance of inertia and viscous forces yields the typical value

$$h \sim \frac{H}{\mathrm{Re}^{1/2}\delta} \tag{16}$$

for the vertical length scale h.

C. Transition between the viscous and the advective regimes

The transition between the viscous regime and the advective regime is characterized by a change in the scaling of the Reynolds number as a function of the forcing. In this transition,

$$\mathrm{Re} \sim \frac{\mathrm{Ch}^{1/2}}{\delta} \sim \frac{\mathrm{Ch}}{\pi^2}, \tag{17}$$

which implies that the transition occurs when

$$\mathrm{Re}\delta^2 \sim \mathrm{Ch}^{1/2}\delta \sim \pi^2. \tag{18}$$

Note that, at this point, the critical value for the length scale h,

$$h \sim \frac{H}{\pi}, \tag{19}$$

can be obtained by comparing the magnitudes of the viscous forces in the advective and viscous regimes.

It is then convenient to define the normalized length scale

$$h^* = \frac{\pi h}{2}, \tag{20}$$

which can be regarded as the thickness of the boundary layers that form next to the bottom and the lid in the advective regime. This would imply that the transition occurs when the thickness of the boundary layer h^* is of the same order of half the total depth H, i.e., when

$$\frac{h^*}{H} \sim \frac{\pi}{2\mathrm{Re}^{1/2}\delta} \sim \frac{1}{2}, \tag{21}$$

and that in the advective regime, the thickness of the boundary layer h^* is smaller than half the total fluid depth.

IV. EXPERIMENTAL RESULTS

Figure 3(a) shows characteristic flow lines tangential to the instantaneous horizontal velocity components in the measurement plane for $\mathrm{Ch} = 1.3\times10^3$ and $\delta = 0.067$. As can be seen, the forcing generates a dipolar structure with a symmetry axis $y = 0$. Apparently, for this value of Ch, the dipole is also nearly symmetric with respect to the line $x = 0$.

Figure 3(b) shows the flow lines for $\mathrm{Ch} = 8.8\times10^5$, with the other parameters unchanged. A clear difference is observed between the flow lines in Figs. 3(a) and 3(b). In particular, the

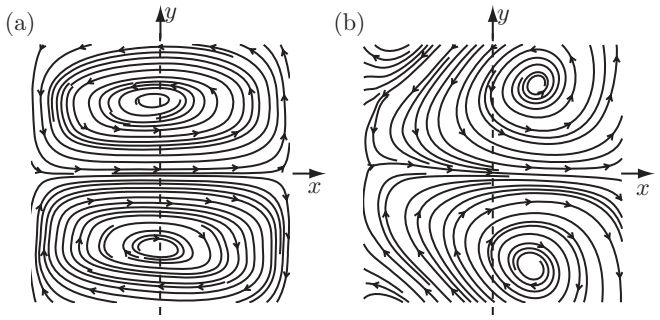

FIG. 3. Flow lines tangential to the horizontal velocity components at mid-depth in the central 30×30 cm^2 region of the tank for (a) Ch $= 1.3 \times 10^3$, (b) Ch $= 8.8 \times 10^5$, and $\delta = 0.067$. The dashed line represents the line $x = 0$.

flow lines for strong forcing spiral out of the vortex cores, in contrast with the flow lines for weak forcing, which are closed. This suggests that there is a strong horizontal divergence for large Ch values. This divergence is due to pumping of fluid from the Bödewadt boundary layers at the bottom and at the lid to the inside of the vortex cores [20]. In addition, there is a strong asymmetry with respect to the line $x = 0$ for Ch $= 8.8 \times 10^5$. This asymmetry can be seen, for example, in the positions of the centers of the two cells which are no longer close to $x = 0$ but displaced in the positive x direction.

To quantify some of the differences in the flow at different values of the forcing, we focus on $\tilde{u}(x)$, the velocity distribution along the symmetry axis of the dipolar structure at $y = 0$. Figure 4 shows the velocity distributions $\tilde{u}(x)$ for different values of Ch and $\delta = 0.04$. The magnitude of $\tilde{u}$ increases with increasing Ch value, and the asymmetry in this velocity distribution with respect to $x = 0$ becomes more pronounced for large Ch values.

Measured values of the Reynolds number Re, based on (5), are plotted in Fig. 5 as a function of the Chandrasekhar number Ch for different values of the aspect ratio δ. The axes have been rescaled with δ^2, and as can be seen, the curves for the different values of δ collapse. Furthermore, the experimental results are compared with the theoretical predictions $\mathrm{Re} \sim \mathrm{Ch}/\pi^2$ and $\mathrm{Re} \sim \mathrm{Ch}^{1/2}/\delta$. The graph clearly shows the existence of the two characteristic scaling regimes: (i) $\mathrm{Re} \sim \mathrm{Ch}/\pi^2$ for $\mathrm{Ch}^{1/2}\delta < \pi^2$ and $\mathrm{Re}\delta^2 < \pi^2$, where the inertia forces can be neglected, and (ii) $\mathrm{Re} \sim \mathrm{Ch}^{1/2}/\delta$ for $\mathrm{Ch}^{1/2}\delta = \mathrm{Re}\delta^2 > \pi^2$,

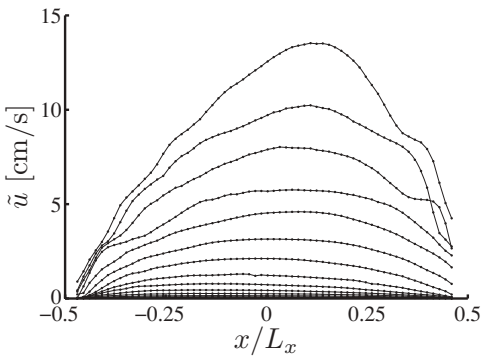

FIG. 4. Measured velocity distributions $\tilde{u}(x)$ at $y = 0$ for different Ch values and $\delta = 0.04$.

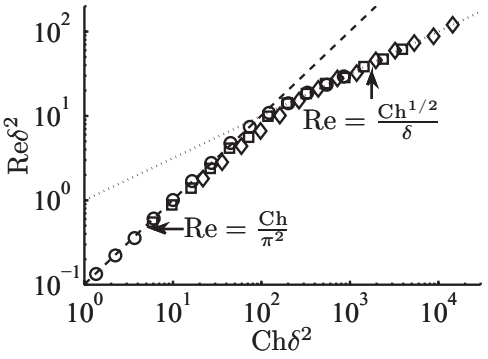

FIG. 5. Magnitude of the response of the flow as a function of the forcing. Measured values of $\mathrm{Re}\delta^2$ as a function of the parameter $\mathrm{Ch}\delta^2$ for various values of Ch, and $\delta = 0.040$ (◯), $\delta = 0.067$ (□), and $\delta = 0.107$ (◇). The dashed line represents $\mathrm{Re} = \mathrm{Ch}/\pi^2$ (viscous regime) and the dotted line represents $\mathrm{Re} = \mathrm{Ch}^{1/2}/\delta$ (advective regime). The intersection of the dashed and dotted lines represents the transition point $\mathrm{Re}\delta^2 = \mathrm{Ch}^{1/2}\delta = \pi^2$.

where the Lorentz and the inertia forces are of the same order. Furthermore, a rather sharp transition is observed at $\mathrm{Re}\delta^2 \sim \mathrm{Ch}^{1/2}\delta \sim \pi^2$.

The collapse of the curves in Fig. 5 for different δ values indicates that the only two relevant parameters of the problem are $\mathrm{Ch}\delta^2$, as the input parameter, and $\mathrm{Re}\delta^2$, as the response parameter. Note that $\mathrm{Re}\delta^2$ is inversely proportional to the square of the boundary layer thickness h^* defined in (20). This suggests that the dynamics of the flow are governed by the boundary layer dynamics. In a recent study of decaying shallow swirl flows [21], it was shown that such flows are also characterized by the nondimensional parameter $\mathrm{Re}\delta^2$.

It can also be observed in Fig. 5 that for the deepest layer ($\delta = 0.107$), there is a larger deviation with respect to the curve $\mathrm{Re} = \mathrm{Ch}/\pi^2$ as compared to the results from experiments with shallower layers. This deviation can be explained by the larger importance of horizontal viscous diffusion compared to the vertical viscous diffusion as the depth of the layer is increased.

The existence of the two scaling regimes is a very robust characteristic of the flow studied in the present article: the same scaling was found when considering additional velocity data at other locations instead of only the velocity along the symmetry axis of the dipole at $y = 0$.

To quantify the asymmetry in the flow, we define the ratio of the Reynolds number Re^+ characterizing the flow at $x > 0$ and the Reynolds number Re^- for $x < 0$:

$$q \equiv \frac{\mathrm{Re}^+}{\mathrm{Re}^-} = \frac{\int_0^{L_x/2} \tilde{u}(x)\,dx}{\int_{-L_x/2}^{0} \tilde{u}(x)\,dx}, \tag{22}$$

which is plotted in Fig. 6 as a function of $\mathrm{Ch}\delta^2$ for $\delta = 0.04$, 0.067, and 0.0107. A reasonably good collapse of the experimental data for the three values of δ is observed, supporting the previous result that the flow only depends on the values of $\mathrm{Ch}\delta^2$. For $\mathrm{Ch}\delta^2 \lesssim 30$, the asymmetry parameter $q \approx 1$. This suggests that the flow is almost symmetric with respect to $x = 0$. As the value of Ch increases, q sharply increases until $\mathrm{Ch} \approx 10^3$. For $\mathrm{Ch} \gtrsim 10^3$, the asymmetry in the

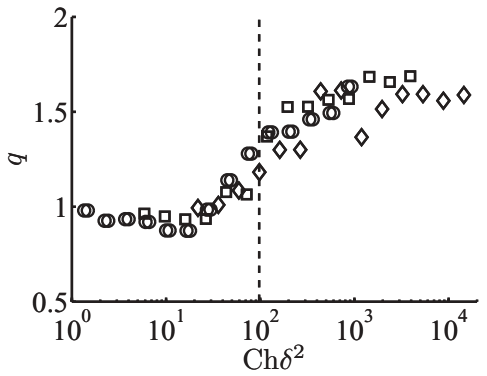

FIG. 6. Measured asymmetry parameter q as a function of the input parameter $\mathrm{Ch}\delta^2$ for $\delta = 0.04$ (◯), $\delta = 0.067$ (□), and $\delta = 0.107$ (◇). The dashed line represent the transition value $\mathrm{Ch}\delta^2 = \pi^4$.

flow remains almost constant with $q \approx 1.7$. This saturation of q is probably due to the presence of the lateral boundary at $x = L_x/2$ since the maximum of $\tilde{u}(x)$ must remain at a finite distance away from this boundary because $\tilde{u}(L_x/2) = 0$.

The transition between $q \approx 1$ and $q \approx 1.7$ corresponds to the change in scaling between the viscous and the advective regimes shown in Fig. 5. Even though the change in the asymmetry is smoother than the change in the scaling, it can be concluded that the increase in asymmetry is due to advection, which gradually becomes more important as the forcing magnitude is increased.

V. IMPLICATIONS FOR PREVIOUS AND FUTURE WORK

Shallow flows are generally modeled with the quasi-two-dimensional Navier-Stokes equation [4]:

$$\frac{\partial \boldsymbol{v}_H}{\partial t} + (\boldsymbol{v}_H \cdot \boldsymbol{\nabla}_H)\boldsymbol{v}_H = -\frac{1}{\rho}\boldsymbol{\nabla}_H p + \lambda \boldsymbol{v}_H + \frac{\boldsymbol{f}}{\rho}, \qquad (23)$$

and the continuity equation

$$\boldsymbol{\nabla}_H \cdot \boldsymbol{v}_H = 0, \qquad (24)$$

where $\boldsymbol{v}_H$ is the horizontal velocity, $\boldsymbol{\nabla}_H$ is the horizontal gradient operator, $\boldsymbol{f}$ is an external force, and λ is a constant known as the *external friction parameter* or the *Rayleigh friction parameter*. Over the years, many different expressions have been suggested for the friction parameter: $\lambda = 2\nu/H^2$ [22], $\lambda = \pi^2\nu/(4H^2)$ [21,23], or $\lambda = 2\kappa\nu/H^2$, where κ is a fitting parameter that depends on the velocity field [4,9,13]. In these cases, H is the total depth of the fluid between a solid bottom and a free surface instead of between a solid bottom and a solid lid, as considered in the current article. In general, a good agreement has been found between theory and experiments. These observations have led to believe that the use of a linear damping term to parametrize the effect of bottom friction in shallow flows is well supported.

However, in the current article, we have found the well-defined limit $\mathrm{Ch}\delta^2 = \pi^4$ for the use of (23) and (24) to model electromagnetically forced shallow flows. Above this limit, the damping rate due to bottom friction depends on the thickness of the boundary layer which, in turn, depends on the magnitude and distribution of the horizontal flow velocity.

Previous experiments have been usually carried out in fluid layers with a depth $H \approx 0.2$–0.3 cm, while the fluid depth is one order of magnitude larger in the experiments presented in the current article. Despite this difference, the corresponding nondimensional parameters have similar values, implying that the flows are dynamically similar.

In previous experiments on electromagnetically shallow flows, only the linear relationship between the forcing and the velocity has been reported, even though small deviations for strong forcing were also observed (see, e.g., Ref. [10]). This implies that these experiments where performed mostly within the viscous regime, thus supporting previous experimental results.

Due to the success of (23) and (24) in describing shallow flows, this system of equations has been solved numerically to model an electromagnetically forced array of vortices in a shallow layer of an electrolyte [24]. In these simulations, the magnitude of the forcing was varied while λ was kept constant. For small forcing magnitudes, a good agreement with laboratory experiments was obtained, and a threshold equivalent to $\mathrm{Ch}\delta^2 = \pi^4$ at which the vortices changed shape was observed. However, for stronger forcing magnitudes the numerical simulations started to differ significantly from the experimental data. This discrepancy can be easily explained since above the threshold $\mathrm{Ch}\delta^2 = \pi^4$ the damping rate depends on the forcing, and λ is no longer a constant.

In addition, for $\mathrm{Ch}\delta^2 > \pi^4$, the flow lines tangential to the horizontal velocity describe spirals originating at the vortex cores. This shape suggests a strong horizontal divergence, in disagreement with (24). In fact, it is for this type of flows with curvilinear streamlines and an additional secondary motion that Ponomarev *et al.* [14] proposed that $\mathrm{Re} \propto \mathrm{Ch}^{2/3}$. However, in our experiments, a clear regime with this scaling was not observed.

It has been noticed in previous work that experiments in a single shallow layer have some shortcomings for the study of two-dimensional turbulence. This motivated experiments in a two-layer configuration [25,26], which were later considered as ideal to study two-dimensional flows. The problem of the response of the flow to EM forcing in these two-layer experiments is certainly more complex than in a single layer, e.g., there is a larger number of nondimensional parameters, a deformable interface, and a deformable free-surface. However, the results presented in the current article indicate that there is also a dynamical limit for considering a two-layer shallow-flow as quasi-two-dimensional.

VI. CONCLUSIONS

We studied experimentally the response of a generic electromagnetically forced flow. This response was quantified by measuring the Reynolds number Re as a function of the Chandrasekhar number Ch (the ratio of Lorentz forces to viscous forces). We found two scaling regimes: $\mathrm{Re} \sim \mathrm{Ch}/\pi^2$ (viscous regime) and $\mathrm{Re} \sim \mathrm{Ch}^{1/2}\delta^{-1}$ (advective regime), with a transition at $\mathrm{Re}\delta^2 \sim \mathrm{Ch}^{1/2}\delta \sim \pi^2$. This scaling is in good agreement with our theoretical predictions.

The transition between the two regimes is related to a qualitative change of the vertical velocity profile: from a Poiseuille-like profile in the viscous regime to a profile

composed, in the advective regime, of an inviscid interior and two boundary layers, one at the bottom and one at the lid, each with a thickness $h^* = \pi H/(2\mathrm{Re}^{1/2}\delta)$. This transition marks the upper limit for the magnitudes of the forcing and the velocity where the quasi-two-dimensional Navier-Stokes equations (23) and the two-dimensional continuity equation (24) can be used to model shallow flows. Furthermore, it was found that the flow is characterized by a single parameter $\mathrm{Re}\delta^2$. Such a conclusion had already been reached by Dolzhanskii [27] for the viscous regime where the flow is described by (23) and (24). However, it has been shown in the current article that this dependence extends to the advective regime.

In the particular case of the dipolar structure studied here, nonlinear effects are reflected in the form of an asymmetry due to the self-advection of the two vortices composing the dipole, as it had been previously observed [13,15]. These nonlinear effects, in the form of vortex-vortex interactions, can be already observed for $\mathrm{Ch}\delta^2 \gtrsim 30$ as inertia forces become increasingly important, and they are predominant in the advective regime when $\mathrm{Re} \sim \mathrm{Ch}^{1/2}\delta^{-1}$, i.e., for $\mathrm{Ch}\delta^2 > \pi^4$.

The current article presents new insight into the structure and dynamics of electromagnetically forced flows in a shallow layer of electrolyte. The results presented can serve as a guideline for future experimental and numerical work on, for example, shallow flows, quasi-two-dimensional turbulence, or the stability of quasi-two-dimensional spatially periodic flows. Another interesting line for future research is the study of the response of the flow to the electromagnetic forcing in other conductive fluids such as liquid metals, which are of interest in metallurgical processing applications.

[1] P. Tabeling, S. Burkhart, O. Cardoso, and H. Willaime, Phys. Rev. Lett. **67**, 3772 (1991).

[2] H. J. H. Clercx, G. J. F. van Heijst, and M. L. Zoeteweij, Phys. Rev. E **67**, 066303 (2003).

[3] R. A. D. Akkermans, L. J. P. Kamp, H. J. H. Clercx, and G. J. F. van Heijst, Europhys. Lett. **83**, 24001 (2008).

[4] F. V. Dolzhanzkii, V. A. Krymov, and D. Yu. Manin, J. Fluid Mech. **241**, 705 (1992).

[5] L. Rossi, J. C. Vassilicos, and Y. Hardalupas, J. Fluid Mech. **558**, 207 (2006).

[6] G. A. Voth, G. Haller, and J. P. Gollub, Phys. Rev. Lett. **88**, 254501 (2002).

[7] P. A. Davidson, Annu. Rev. Fluid Mech. **31**, 273 (1999).

[8] S. Kenjereš, Phys. Rev. E **78**, 066309 (2008).

[9] N. F. Bondarenko, M. Z. Gak, and F. V. Dolzhanskiy, Izv. Acad. Sci., USSR, Atmos. Ocean. Phys. **15**, 711 (1979).

[10] P. Tabeling, B. Perrin, and S. Fauve, Europhys. Lett. **3**, 459 (1987).

[11] T. Dauxois, S. Fauve, and L. Tuckerman, Phys. Fluids **8**, 487 (1996).

[12] A. Thess, Phys. Fluids A **4**, 1385 (1992).

[13] S. D. Danilov and V. A. Dovzhenko, Izv. Atmos. Ocean. Phys. **31**, 593 (1996).

[14] V. M. Ponomarev, A. A. Khapaev, and I. G. Yakushkin, Izv. Atmos. Ocean. Phys. **44**, 45 (2009).

[15] A. Figueroa, F. Demiaux, S. Cuevas, and E. Ramos, J. Fluid Mech. **641**, 245 (2009).

[16] The kinematic viscosity was measured for the solution used in the experiments at working temperature 21°C using a capillary viscometer 501 13 from Schott Instruments.

[17] S. Chandrasekhar, *Hydrodynamic and Hydromagnetic Stability* (Clarendon Press, Oxford, 1961), p. 7.

[18] R. Klein, A. Pothérat, and A. Alferenok, Phys. Rev. E **79**, 016304 (2009).

[19] A. M. Batchaev, Zh. Prikl. Mekh. Tekh. Fiz. **4**, 85 (1990).

[20] U. T. Bödewadt, Z. Angew. Math. Mech. **20**, 241 (1940).

[21] M. Duran-Matute, L. P. J. Kamp, R. R. Trieling, and G. J. F. van Heijst, J. Fluid Mech. **648**, 471 (2010).

[22] F. V. Dolzhanskii, V. A. Krymov, and D. Yu. Manin, Sov. Phys. Usp. **33**, 495 (1990)

[23] A. E. Hansen, D. Marteau, and P. Tabeling, Phys. Rev. E **58**, 7261 (1998).

[24] Y. Nakamura, J. Phys. Soc. Jpn. **65**, 1666 (1996).

[25] J. Paret and P. Tabeling, Phys. Rev. Lett. **79**, 4162 (1997).

[26] M. G. Shats, H. Xia, and H. Punzmann, Phys. Rev. E **71**, 046409 (2005).

[27] F. V. Dolzhanskiy, Izv. Atmos. Ocean. Phys. **23**, 262 (1987).